JTTEE5 12:226-233

Peer Reviewed

Effect of Uniaxial Pressure on Ultrasound Velocities and Elastic Moduli in Plasma-Sprayed Ceramics

M. Landa, F. Kroupa, K. Neufuss, and P. Urbánek

(Submitted 23 November 2001; in revised form 28 February 2002)

Microcracks and thin voids in plasma-sprayed ceramics are known to be responsible for elastic anisotropy and for small values of elastic stiffness constants (measured at small stresses), compared with well-sintered materials. The increase of ultrasound velocities with increasing uniaxial pressure up to 300 MPa in three types of plasma-sprayed ceramics was measured in two directions. The corresponding elastic stiffnesses increased from 1.4 to 4.7 times. The experimental results were explained by closing of intrasplat microcracks and intersplat thin voids by uniaxial pressure.

Keywords compressive stresses, elastic stiffnesses, microcracks and thin voids closure, plasma-sprayed ceramics, ultrasound velocities

1. Introduction

Coatings and freestanding parts prepared by plasma spraying (or by other types of thermal spraying) have much lower Young's moduli than well-sintered materials. Moreover, they have different Young's moduli in the directions parallel and perpendicular to the surface. These effects are more pronounced in ceramics than in metals and have been shown in a number of experiments performed at low stresses.[1] They are associated with the complex microstructure of plasma-sprayed materials, which consist of irregular thin lamellae called splats and voids of various types, usually with the total porosity volume between 5% and 15%. The voids can be divided into four types: irregular pores between the splats, thin voids (unbounded regions) between the splats, spherical pores inside the splats, and microcracks inside the splats.

Thin voids between the splats and microcracks inside the splats with large total areas have the most important effect on the elastic properties. These two types of defects have different orientations with respect to the spraying plane. For the spraying direction x_3, the splats are approximately parallel with the spraying plane x_1x_2 (Fig. 1), and

1) Thin voids between the splats, formed as unbounded regions along the splat interfaces, are approximately parallel to the spraying plane x_1x_2 and will be called intersplat (or horizontal) thin voids.
2) Microcracks approximately perpendicular to the spraying plane x_1x_2, formed inside the splats during their rapid cooling after solidification, are called intrasplat (or vertical) microcracks.

M. Landa and **P. Urbánek,** Institute of Thermomechanics, ASCR, Dolejskova 5, 182 00 Prague 8, Czech Republic; and **F. Kroupa** and **K. Neufuss,** Institute of Plasma Physics, ASCR, Za Slovankou 3, 182 21 Prague 8, Czech Republic. Contact e-mail: ml@it.cas.cz.

The thin voids and microcracks contribute only to a small part of the total porosity; however, they have the main influence on the decrease of Young's moduli by small elastic openings and partial closings of their faces. The intersplat thin voids lead to the decrease of Young's modulus E_3 in the spraying direction x_3 while the intrasplat microcracks lead to the decrease of Young's moduli E_1 in the directions x_1 lying in the x_1x_2 plane.

The small values of E_3 and E_1 were, in principle, well explained in theoretical papers[2-5] where the thin voids and microcracks are modeled as flat hollow rotational ellipsoids in an elastic isotropic continuum characterized by Young's modulus E_0

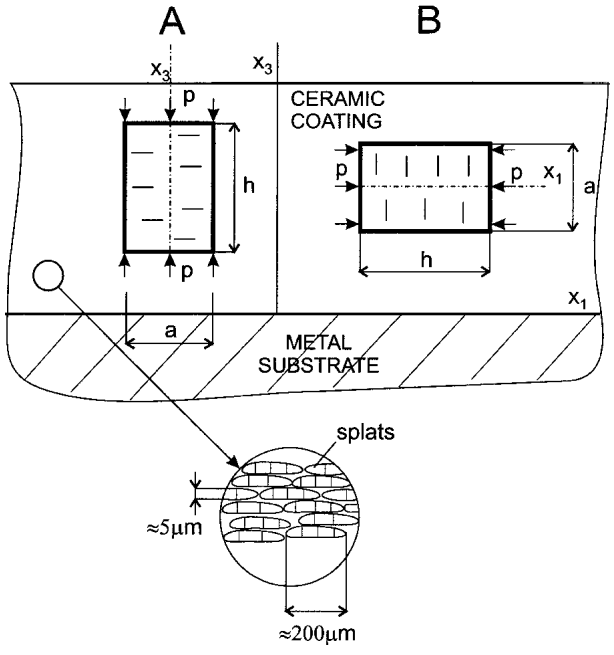

Fig. 1 Specimens of type A and B (of dimensions $a \times a \times h$) cut from a ceramic coating. The influential intersplat (horizontal) thin voids in specimen A and intrasplat (vertical) microcracks in specimen B are depicted schematically.

and Poisson's ratio ν_0 (corresponding to a well-sintered polycrystalline material). For the normals to the intrasplat cracks randomly distributed in the x_1x_2 planes, the body is anisotropic, of transverse isotropy with respect to the x_1x_2 plane, characterized by 5 independent elastic constants. The thin voids and microcracks are assumed to be sufficiently opened so that their surfaces do not come into contact under small compressive stresses and the same values of Young's moduli under tension as well as under compression follow.[2-5] These papers are based on the linear theory of elasticity, and for given dimensions and densities of thin voids and microcracks, the elastic stiffnesses are derived as constants independent of stress.

A possible effect of higher compressive stresses on Young's moduli E_3 and E_1 of thermally sprayed materials has recently been discussed.[6] The surfaces of a thin void or microcrack will come into contact under compressive stress p_c given as $p_c/E_0 = k(b/r)$ where b/r is the thin void or microcrack aspect ratio, and the value of parameter k ≅ 0.5 is slightly dependent on their forms. Therefore, with increasing value of compressive stresses σ, more and more thin voids and microcracks become elastically closed and the moduli E_3 and E_1 should approach at very high pressures the value ≈0.8 E_0 (the decrease from E_0 to ≈0.8 E_0 is due to residual porosity).

The elastic behavior of sprayed materials under compressive stresses was recently modeled within the framework of the nonlinear anisotropic theory of elasticity.[7]

It should be pointed out that a similar effect is well known and important in geophysics as the effect of hydrostatic or uniaxial pressure on the velocity of elastic waves and on the elastic stiffnesses of rocks containing cracks.[8-10]

An increase of Young's modulus E_1 of the order of ten percent in a plasma-sprayed zircon ($ZrSiO_4$) coating on a Ti-alloy substrate was found from bending experiments even at small compressive stresses in the coating, σ ≅ −20 MPa.[11]

Systematic measurements of the dependence of Young's moduli E_1 and E_3 of various plasma-sprayed ceramic materials in a wide range of compressive stresses seem to be useful.

In this paper, the dependence of elastic stiffnesses c_{11} and c_{33} on compressive stresses for three plasma-sprayed ceramic materials is studied. The basic experimental method is the measurement of ultrasound velocity in freestanding specimens of sufficiently large dimensions in dependence on uniaxial compressive stress, in the widest possible range of elastic deformations. From the measured ultrasound velocities, the dependence of elastic stiffnesses c_{11}, c_{33} on uniaxial pressure is evaluated.

2. Experimental

2.1 Specimens

Three types of plasma-sprayed ceramics, gray alumina, zircon, and olivine (Table 1), were prepared from powders by plasma spraying, using the water stabilized plasma gun PAL 160.[12] Coatings of thickness 11 mm were formed on steel substrates. Freestanding ceramic plates were then prepared by separation of the coatings from the substrates by a special thermal treatment. Specimens in the form of prisms of nominal dimensions 8 × 8 × 9 mm^3 were manufactured from these plates by diamond saw cutting. Specimens of two orientations were chosen: specimens of type A had the axis (in the direction of the dominant direction h = 9 mm) in the x_3 direction perpendicular to the plate plane, specimens of type B had the axis in the x_1 direction parallel to the plate plane (Fig. 1). Three specimens for each orientation were prepared. All specimens had the microstructure typical of plasma-sprayed ceramics, as documented in Fig. 2 for gray alumina. The bases of the prisms (of dimensions 8 × 8 mm^2) were ground to become as plan parallel as possible.

Well-sintered specimens of commercial white alumina OXAL 241-R (Jiskra, Tabor, Czech Republic) were used for calibration and comparison with the results for plasma-sprayed ceramics (Table 1). They contained 95.5% pure Al_2O_3 and 4.5% of other oxides forming the glass phase along the grain boundaries. Their porosity was less then 1% and they contained no microcracks. The specimens were of a cylindrical shape of diameter 7.5 mm and height h = 9 mm.

Table 1 Tested Materials

Name	Chemical Composition	Total Porosity, %	ρ, kg/m^3
Gray alumina	psd: Al_2O_3 + 3% TiO_2	12.8	3360
Zircon	psd: $ZrSiO_2$	17.2	3656
Olivine	Initial: 49.50% MgO, 40.81% SiO_2, 7.00% Fe_2O_3 + others psd: 50.90% MgO, 40.30% SiO_2, 6.73% Fe_2O_3 + others	6.3	3048
Oxal 241-R	sintered: 95.5% Al_2O_3	<1	3649

psd, plasma-sprayed deposition

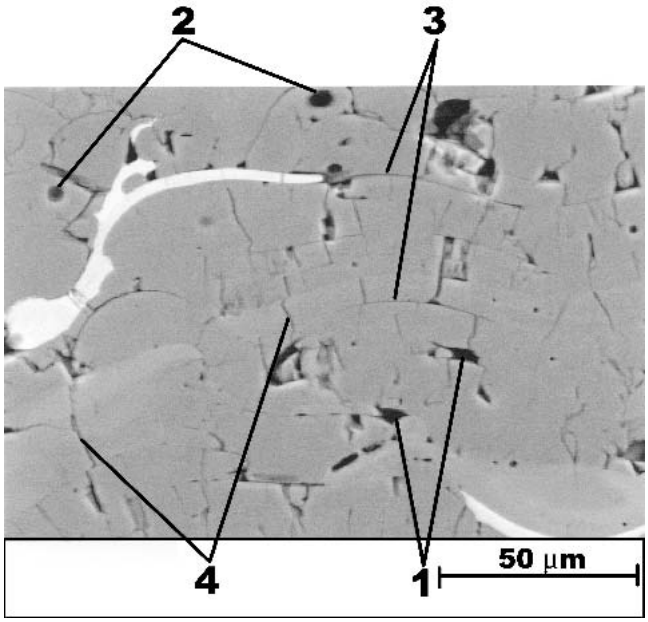

Fig. 2 SEM microstructure of plasma-sprayed gray alumina (Al_2O_3 + 3%TiO_2). White areas: TiO_2; 1, Irregular pores between the splats (some larger black areas may correspond to pull-outs); 2, Spherical pores inside the splats; 3, Intersplat (horizontal) thin voids; 4, Intrasplat (vertical) microcracks

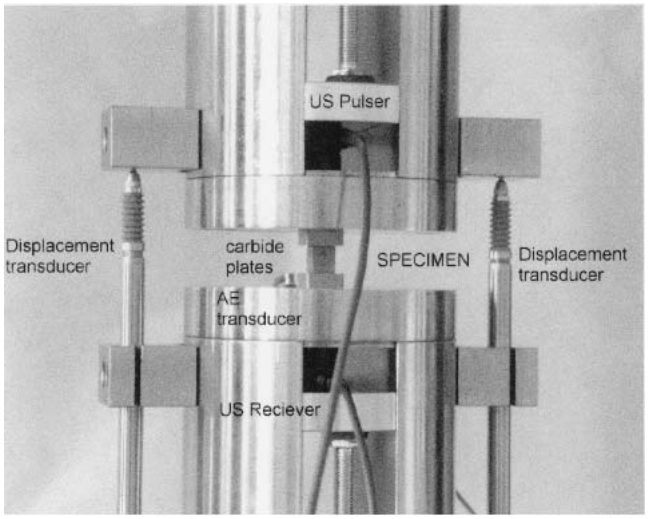

(a)

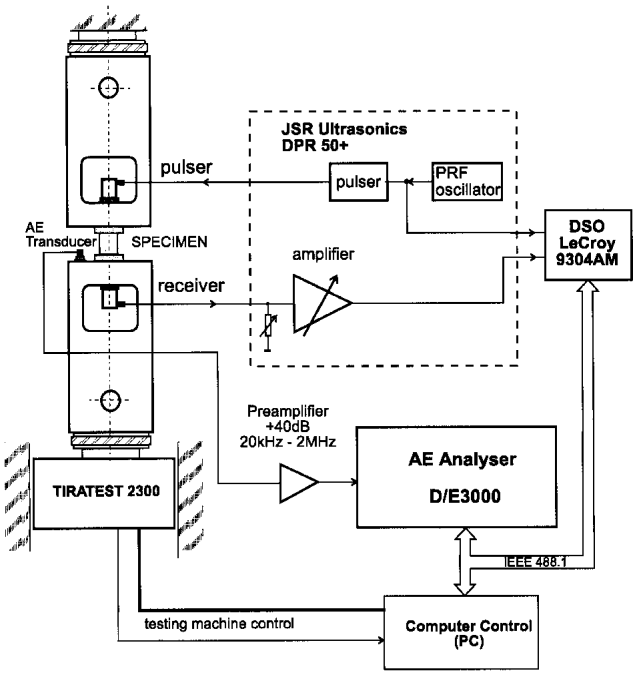

(b)

Fig. 3 Experimental setup for the measurement of ultrasound velocities under uniaxial pressure: **(a)** specimen in the test machine, **(b)** the block scheme of the experimental arrangement

2.2 Measurement of Ultrasound Velocity Under Uniaxial Pressure

The compression tests were carried out at room temperature on the electromechanical test machine Tiratest 2300, 100kN (VEB Thüringer Industriewerk, Rauenstein, Germany). The loading plattens were designed to allow the ultrasonic measurements on the loading axis (Fig. 3a). The specimens were clamped between two sintered tungsten carbide disks (cutting tips $12.7 \times 12.7 \times 4.808$ mm^3 with Ti coating, Diadur, Sumperk, Czech Republic) to protect from the sinking of specimens into the steel plates. The friction on the contacting interfaces was decreased by the Ti coating. The displacement was measured by two inductive transducers.

The compression tests on the prismatic specimens were performed in two steps:

1) The acoustic emission (AE) activity (count rate dN_c/dt) was monitored during the first loading cycle to find the maximum loading level, which did not cause significant damage to the tested material. This first cycle is marked as "first" in the p-ε plots where p is the pressure and ε the compressive deformation (Fig. 4a,b). A partial unloading was performed to observe the existence of the Kaiser effect.[13] The bottom plots in Fig. 4(c) and (d) show the history of loading and AE activity. The loading is up to the moment when some AE appears. Unloading and reloading up to the previous compression level are not accompanied with AE (Fig. 4c). After crossing the previous loading maximum (Fig. 4d), other irreversible changes in the material are initiated and indicated by AE.
2) During the next cycle, the loading was interrupted step by step and ultrasonic measurements were applied (in the p-ε plots, the loading stops are marked by circles). These loading cycles are noted by "next" in Fig. 4(a) and (b).

AE is an important tool for detecting the irreversible changes in brittle materials. The AE sensor was placed on the bottom-loaded plate. The AE analyzer with the audio monitor was also used.

The transmission pulse technique was used for ultrasonic measurements (the ultrasonic transducers type "gamma," 5 MHz/0.25″, KB-Aerotech, Lewistown, PA; exciting and detecting longitudinal waves, the Pulser/Receiver system DPR 50+, JSR Ultrasonics, Pittsford, NY; and the digital storing oscilloscope 9304AM, LeCroy Corp., Chestnut Ridge, NY).

A reference measurement was performed on the inserted third tungsten carbide disk (thickness, 4.808 mm) to eliminate the influence of the loading system deformation.

The whole transmitted pulse was recorded and the times of flight (TOFs) were evaluated by two techniques: the threshold level crossing and the cross-correlation functions.[14] The difference between the results is a measure of the wave dispersion. The wave velocity in the stress-free state was measured by the pulse-echo technique.[15]

The signal amplitude was also evaluated, and the wave attenuation changes during the loading were determined.

The block scheme of the experimental arrangement is shown in Fig. 3(b).

2.3 Evaluation of the Pressure Dependence of Elastic Parameters

From the measured longitudinal ultrasound velocities v_3 (p) for specimens of type A and v_1 (p) for specimens of type B, the dependences of elastic stiffnesses c_{33} and c_{11} on uniaxial pressure p can be calculated,

$$c_{33}(p) = v_3^2(p)\,\rho,\ c_{11}(p) = v_1^2(p)\,\rho \qquad \text{(Eq 1)}$$

where ρ is the volume mass density given in Table 1.

The sintered alumina OXAL is isotropic, $v_3 = v_1$ and $c_{33} = c_{11} = c = E(1-\nu)/[(1+\nu)(1-2\nu)]$.

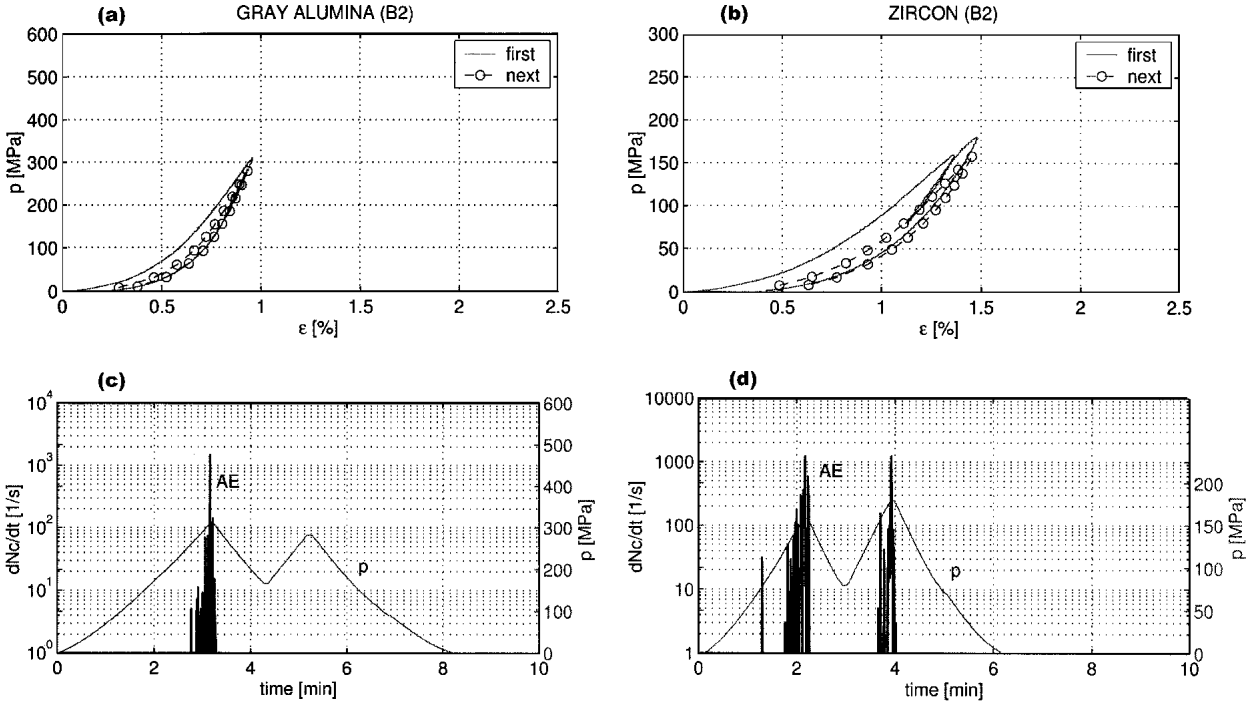

Fig. 4 Monitoring of acoustic emission activity (AE) in **(a, c)** gray alumina and **(b, d)** zircon; (a) loading and unloading curves in the first virgin cycle and the next measuring cycle, (b) the history of loading and AE activity in two different virgin cycles

Table 2 Stress-Free Material Properties

	V_3, m/s		C_{33}, GPa		V_1, m/s		C_{11}, GPa	
Material Type	**Mean**	**STD**	**Mean**	**STD**	**Mean**	**STD**	**Mean**	**STD**
Gray alumina	4293	(24)	61.9	(0.7)	4 230	(197)	60.2	(5.7)
Zircon	1889	(10)	13.0	(0.1)	2 496	(27)	22.8	(0.5)
Olivine	6224	(30)	118.1	(1.1)	3 140	(11)	30.1	(0.2)
Oxal 241-R*	9915	(2)	358.8	(0.1)				

*$V_1 \equiv V_3$ and $C_{11} \equiv C_{33}$.

Young's modulus $E = 0.833c$ can be calculated using the known Poisson's ratio $\nu = 0.25$.

For the anisotropic plasma-sprayed ceramics, the usually used Young's moduli E_3 and E_1 cannot be calculated from the measured elastic stiffnesses c_{33} and c_{11}. For a very rough estimate, the relations $E_3(p) \approx 0.8\, c_{33}(p)$ and $E_1(p) \approx 0.8\, c_{11}(p)$ can be used.[16]

It should be pointed out that, using the ultrasound measurements, only small changes of stresses $\Delta\sigma_{ij}$ are superimposed on the instantaneous stress values σ_{ij} and small changes of elastic strains Δe_{ij} of instantaneous strains e_{ij} are induced. The corresponding constitutive law between the infinitesimal changes of stress and strain can be written in the reduced index notation[16] as

$$d\sigma_i = \sum_{j=1}^{6} c_{ij} de_j$$

where c_{ij} are the instantaneous (called also tangent or current) elastic stiffnesses, which are functions of instantaneous stress values σ_{mn}. For uniaxial compression, $p = -\sigma_{33}$ or $p = -\sigma_{11}$, and compressive deformation, $\varepsilon = -e_{33}$ or $\varepsilon = -e_{11}$, the instantaneous stiffnesses used in Eq 1 can be defined as $c_{33}(p) = dp/d\varepsilon$ and $c_{11}(p) = dp/d\varepsilon$.

3. Experimental Results

The measured ultrasound velocities v_3 and v_1 (averages of values measured on three specimens of the same type) and calculated elastic stiffness constants c_{33} and c_{11} in the four stress-free materials are summarized in Table 2. The values of the volume mass densities ρ are the average mass densities of materials containing pores and microcracks. The same values of ρ were used as a good approximation for calculation of c_{33} and c_{11} in Eq 1 in materials under pressure.

The measured velocities v_3 and v_1 for specimens A and B, respectively, in dependence on uniaxial pressure p are plotted in Fig. 5. Only the results for one typical specimen of each type are given. The measured values for the other two specimens of the same type differ by less than 5%. However, the maximum applied pressures slightly differed and it was difficult to plot the average curve for the three specimens of the same type.

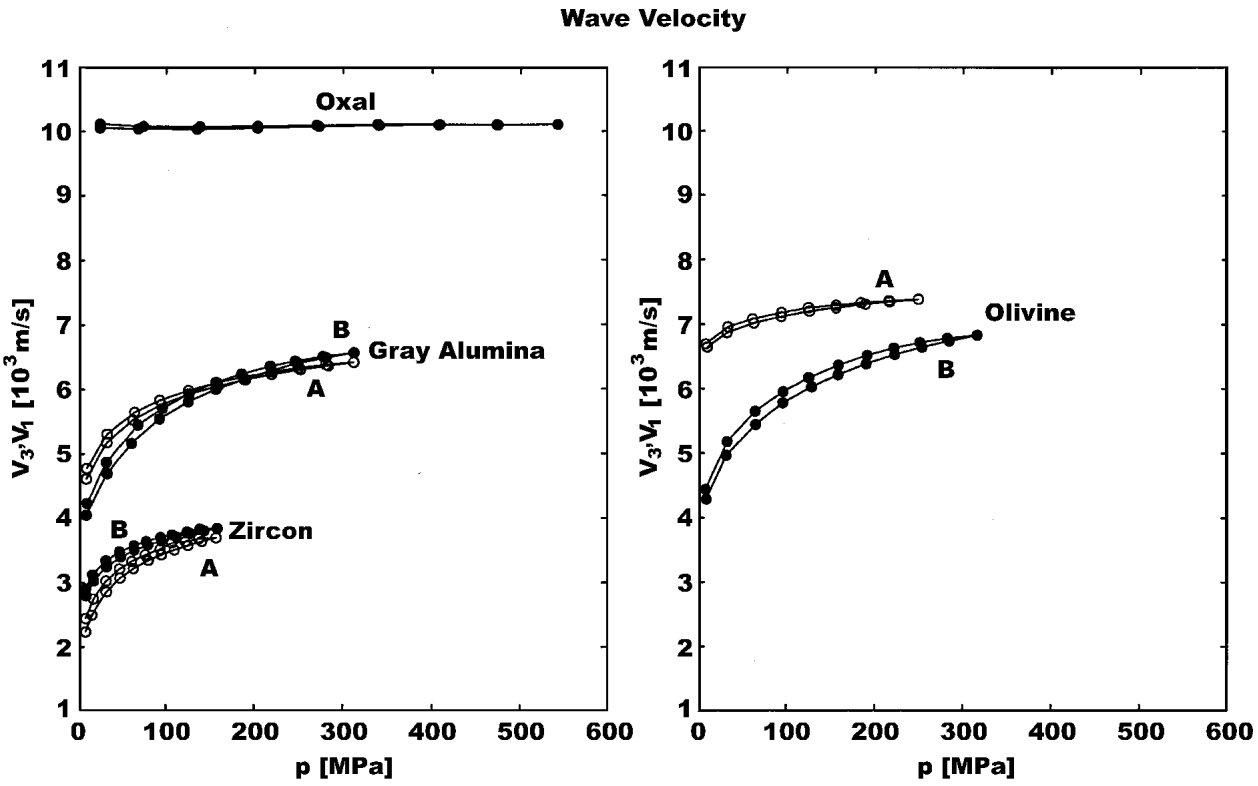

Fig. 5 Dependence of measured ultrasound velocities v_3 (in specimens A) and v_1 (in specimens B) on uniaxial pressure p, for three types of plasma sprayed ceramics. The lower curves were measured during loading, the upper curves during unloading; the results for sintered ceramics OXAL are also included.

As additional information, the measured wave attenuation is shown in Fig. 6.

The instantaneous elastic stiffnesses c_{33} and c_{11}, calculated from Eq 1, in dependence on uniaxial pressure p are plotted in Fig. 7.

4. Discussion

4.1 Pressure Dependence of Elastic Stiffnesses Due to Closure of Microcracks and Thin Voids

A considerable increase of ultrasound velocities and of elastic stiffnesses with increasing uniaxial pressure in plasma sprayed ceramics has been found in Fig. 5 and 7. These effects can be ascribed to closing of microcracks and thin voids under pressure.

The measurement of the wave attenuation in Fig. 6 also supports the idea of closing of microcracks and thin voids. The wave attenuation α is related to the reference material and to the unit length of the wave path,

$$\alpha = (1/h)\ 20 \log [A(p)/A_{ref}(p)],\ \text{dB/mm} \qquad \text{(Eq 2)}$$

where $A_{ref}(p)$ and $A(p)$ are the amplitude of the transmitted pulse in the reference material (the same for OXAL and tungsten carbide) and in the measured plasma-sprayed specimens, respectively. The attenuation in plasma-sprayed materials is due to inhomogeneties, i.e., mainly to microcracks, thin voids, and pores. There is high attenuation (high negative values of α) in specimens at low pressures (with a high density of open microcracks and thin voids) and it decreases with increasing pressure, i.e., with closing of microcracks and thin voids. Figure 6 confirms the decrease of the density of open microcracks and thin voids with pressure. Note, for example, the low density of horizontal thin voids in specimens A of olivine at small stresses, compared with a high density of vertical microcracks in specimens B at small stresses.

The pressure dependence of c_{33} in the A type specimens is due mainly to closing of the horizontal thin voids while the pressure dependence of c_{11} in the B type specimens is governed by closing of the vertical microcracks, as shown in Fig. 1.

The dependences in Fig. 5 and 7 measured during loading (lower curves) and unloading (upper curves) slightly differ. Therefore, the behavior is not purely elastic. This can be explained by the fact that there are not only microcracks or thin voids perpendicular to the compression axis but also some of them forming different angles with this axis. The shear stresses along their planes cause relative displacements of their faces associated with friction and energy absorption. The same effect is known in geophysics from behavior of rocks with cracks under uniaxial pressure.[9] However, under hydrostatic pressure the loading and unloading curves of rocks coincide as no shear stresses act on the cracks.[8]

As expected, the ultrasound velocities and the elastic stiffness constants in the well-sintered ceramics OXAL without mi-

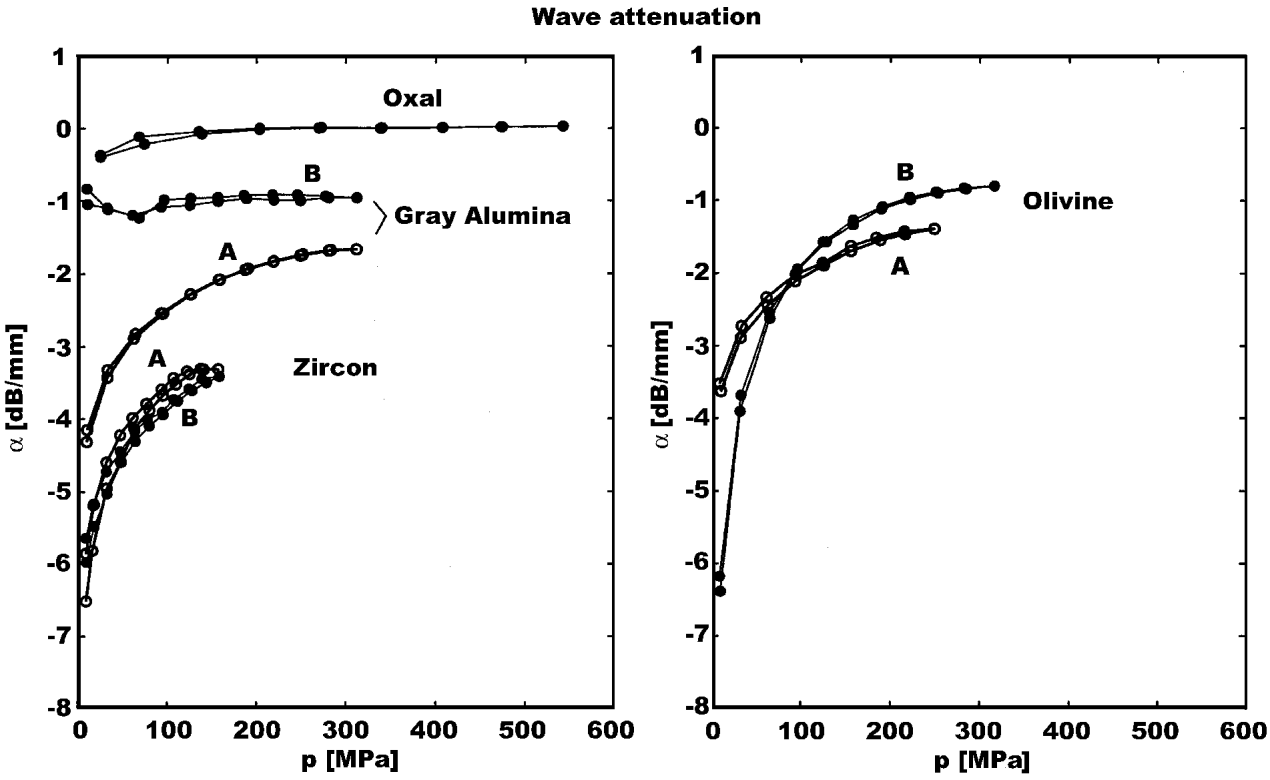

Fig. 6 Change of wave attenuation α with increasing pressure p

crocracks practically do not depend on pressure (Fig. 5 and 7). The small difference between the loading and unloading curves at pressures between 0 and 100 MPa may be explained by the fact that the specimen bases were not exactly plan parallel and the specimen settled at these stresses. A detailed examination of the curve between 100 and 500 MPa shows a slight increase of stiffness, about 0.5%. This is, however, a general effect in solids (without microcracks) due to nonlinear forces between atoms. The measurement of stiffness c_{11} of well-sintered pure isotropic polycrystalline Al_2O_3 under hydrostatic pressure between 0 and 1 GPa showed the increase of c_{11} by 1.4%.[17]

A similar contribution of the nonlinear interatomic forces to elastic stiffnesses takes place also in the plasma-sprayed ceramics. However, at pressures between 0 and 300 MPa, used in this work, this contribution should be smaller than 0.5% and, therefore, negligible with respect to the effect of microcracks and thin voids.

4.2 Differences Between the Three Types of Ceramics

Some differences between the three types of plasma sprayed ceramics can be observed.

For gray alumina and zircon, the curves for c_{33} and c_{11} (Fig. 7) are close and, therefore, the elastic anisotropy of these materials is small and does not change much with pressure. On the other hand, for olivine $c_{33} > c_{11}$ and the material is strongly anisotropic; however, the anisotropy decreases with pressure p. This may be caused by the fact that the sprayed olivine is mostly in the glass phase and good contacts between the splat interfaces develop so that the density of horizontal thin voids is small. Therefore, the value of c_{33} at small stresses is relatively large and the dependence of c_{33} on pressure is weak.

The magnitude of increase of c_{33} and c_{11} from small values at small stresses (given in Table 2) to the maximum values at the highest exerted pressures (Fig. 7) is different for different types of ceramics.

For gray alumina, the increase from the values at zero pressure, $c_{33}(0) \cong c_{11}(0) \cong 60$ GPa, to the values at $p \cong 300$ MPa, $c_{33}(300) \cong c_{11}(300) \cong 140$ GPa, is about 2.3 times.

For zircon, the increase from $c_{33}(0) \cong 13$ GPa and $c_{11}(0) \cong 23$ GPa to $c_{33}(160) \cong 52$ GPa and $c_{11}(160) \cong 54$ GPa, is about 4 and 2.4 times, respectively.

For olivine, the value $c_{33}(0) \cong 118$ GPa is rather high and increases to $c_{33}(250) \cong 166$ GPa, i.e., only 1.4 times. On the other hand, $c_{11}(0) \cong 30$ GPa increases to $c_{11}(310) \cong 142$ GPa, i.e., 4.7 times (indicating that the density of vertical microcracks is high).

It would have been interesting to compare the measured values of stiffnesses c_{33} and c_{11} with the values for well-sintered polycrystalline isotropic materials without voids and microcracks, $c_{33}^0 = c_{11}^0 = c_0$. Unfortunately, it is hardly possible. The main reason is that these three plasma-sprayed ceramic materials have a special metastable phase structure, which develops during the rapid cooling, and that the materials with the same phase structure and without microcracks and voids are not available. Therefore, the values of c_0 (or $E_0 \approx 0.8\ c_0$) cannot be measured.

The shapes of the measured curves in Fig. 7 suggest that saturation has not yet been reached at the maximum pressures used in this work. At even higher pressures, the stiffnesses c_{33} and c_{11}

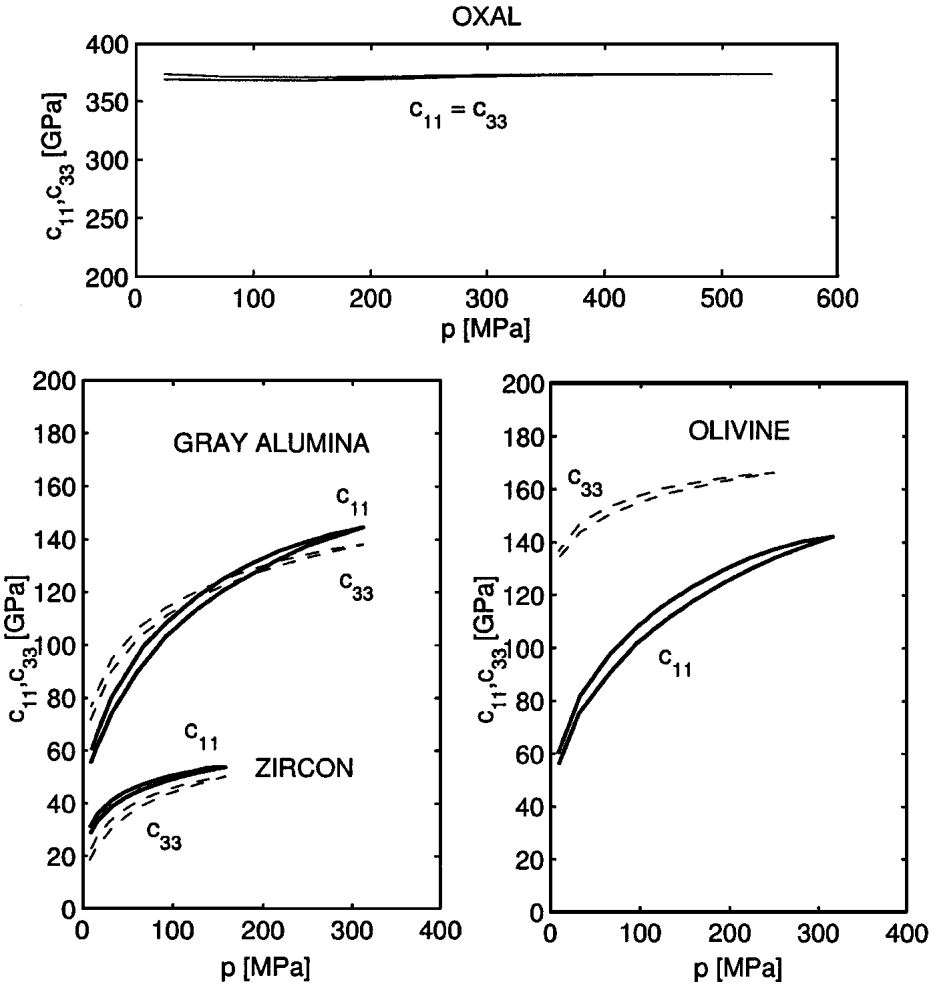

Fig. 7 Dependence of elastic stiffnesses c_{33} (specimens A) and c_{11} (specimens B) on uniaxial pressure p for three types of plasma-sprayed ceramics and for the well-sintered OXAL

are expected to reach the maximum values when all the thin voids, and microcracks are closed and the remaining deficit with respect to c_0 should be due to irregular and spherical pores, which cannot be closed by pressure.

In a simplified discussion of saturation, the values of Young's moduli E of well-sintered ceramics in the stable phase, known from experiments, will be mentioned for comparison.

Well-sintered pure alumina in the usual stable α-phase has a large Young's modulus, $E \cong 400$ GPa. However, in plasma-sprayed gray alumina, metastable phases are formed during rapid solidification with the majority being γ phase. Young's modulus of this phase (without any voids) can be roughly estimated as $E_0 \approx 250$ GPa. Therefore, the saturation effect for gray alumina (Fig. 7) can be expected at pressures rather larger than 300 MPa.

Zircon ($ZrSiO_4$) decomposes partly during the rapid solidification inside the splats into a fine structure composed of small particles of crystalline monoclinic ZrO_2 and glassy SiO_2. Young's modulus of ZrO_2 is $E \cong 210$ GPa and, for glassy SiO_2, $E \cong 75$ GPa.[11] The value E_0 should be between these two values and the measured $c_{33}(160) \approx c_{11}(160) \approx 50$ GPa seem to be far from saturation.

Young's modulus of polycrystalline olivine is $E \approx 200$ GPa. In the plasma-sprayed olivine in a partly glassy phase, a slightly smaller value E_0 can be expected. The measured values $c_{33}(250) \approx 166$ GPa and $c_{11}(310) \approx 142$ GPa seem to be already close to saturation.

However, the AE monitoring used for the determination of the region of pressure causing purely elastic deformation (Fig. 4) suggests that at a higher pressure, approaching saturation, the deformation will no longer be entirely elastic.

5. Conclusions

The dependence of the velocity of the longitudinal ultrasound waves on uniaxial pressure was documented for three types of plasma-sprayed ceramics in two directions.

Acoustic emission was monitored to find the maximum pressure, which did not cause any detectable damage.

The instantaneous elastic stiffnesses c_{33} and c_{11}, calculated from the measured ultrasound velocities, grew with increasing pressure between 0 and 300 MPa in different materials and in different directions 1.4 up to 4.7 times.

These results were explained by elastic closing of the intersplat thin voids and intrasplat microcracks under pressure.

The loading and unloading curves slightly differed, which was explained by relative displacements of the faces of thin voids and microcracks oblique to the compression axes, leading to the appearance of friction forces.

The measurements made for comparison on well-sintered ceramics showed practical independence of ultrasound velocities and elastic stiffness constants on pressure up to 500 MPa.

Acknowledgments

The authors acknowledge the support by GACR grants 106/00/D106 and 106/01/0094. The authors wish to express their thanks to Dr. B. Kolman for the SEM micrographs and to Dr. J. Plesek for reading the manuscript and for fruitful discussions.

References

1. L. Pawlowski: *The Science and Engineering of Thermal Spray Coatings,* J. Wiley, New York, 1995.
2. F. Kroupa: "Effect of Nets of Microcracks on Elastic Properties of Materials," *Kovove Mater.,*1995, *33,* pp. 418-26 (in Czech).
3. F. Kroupa and M. Kachanov: "Effect of Microcracks and Pores on the Elastic Properties of Plasma Sprayed Materials" in *Modelling of Structure and Mechanics of Materials From Microscale to Product,* J.V. Carstensen, T. Leffers, T. Lorentzen, O.B. Pedersen, B.F. Sorensen, and G. Winther, ed., Riso National Laboratory, Roskilde, Denmark, 1998, pp. 325-30.
4. S-H. Leigh and C.C. Berndt: "Modeling of Elastic Constants of Plasma Spray Deposits With Ellipsoid-Shaped Voids," *Acta Mater*., 1999, *47,* pp. 1575-86.
5. I. Sevostianov and M. Kachanov: "Modeling of the Anisotropic Elastic Properties of Plasma-Sprayed Coatings in Relation to Their Microstructure," *Acta Mater*., 2000, *48,* pp. 1361-70.
6. F. Kroupa and J. Dubsky: "Pressure Dependence of Young's Moduli of Thermal Sprayed Materials," *Scripta Mater*., 1999, *40,* pp. 1249-54.
7. F. Kroupa and J. Plesek: "Nonlinear Elastic Behavior in Compression of Thermally Sprayed Materials," *Mater. Sci. Eng. A*, 2002, *328,* pp. 1-7.
8. J.B. Walsh: "The Effect of Cracks on the Compressibility of Rocks," *J. Geophys. Res*., 1965, *70,* pp. 381-89.
9. J.B. Walsh: "The Effect of Cracks on the Uniaxial Elastic Compression of Rocks," *J. Geophys. Res*., 1965, *70,* pp. 399-411.
10. Z. Pros, T. Lokajíček, R. Přikryl, A. Spičak, V. Vajdová and K. Klíma: "Elastic Parameters of West Bohemian Granits Under Hydrostatic Pressure," *Pure and Applied Geophysics,* 1998, *151,* pp. 619-29.
11. V. Harok and K. Neufuss: "Elastic and Inelastic Effects in Compression in Plasma Sprayed Ceramic Coatings," *J. Therm. Spray Technol.,* 2001, *10,* pp. 126-32.
12. M. Hrabovský: "Water-Stabilized Plasma Generators," *Pure Appl. Chem.,* 1998, *70,* pp. 1157-62.
13. A.E. Lord, Jr.: "Acoustic Emission" in *Physical Acoustics,* Vol. 11, R.N. Thurston and A.D. Pierce, ed., Academic Press, New York, 1975, pp. 289-353.
14. M. Landa: "Quantitative Evaluation of Internal Stresses by Ultrasonic Techniques" in *Proceedings of 29th Conference CNDT, Defectoscopy 99,* Hradec Kralove, Nov 17-19, 1999, Czech Society for NDT, Prague, 1999, pp. 29-36.
15. E.P. Papadakis: "The Measurement of Ultrasonic Velocity" in *Physical Acoustics,* Vol. 19, R.N. Thurston and A.D. Pierce, ed., Academic Press, New York, 1990, pp. 81-105.
16. R.F.S. Hearmon: *An Introduction to Applied Anisotropic Elasticity,* Clarendon Press, Oxford, UK, 1961.
17. D.H. Chung and G. Simmons: "Pressure and Temperature Dependences of the Isotropic Elastic Moduli of Polycrystalline Alumina," *J. Appl. Phys*., 1968, *39,* pp. 5316-26.